metals

MDPI

Article

Preparation of Property-Controlled Bi-Based Solder Powders by a Ball-Milling Process

Sang Hoon Kim [1,2], Min Jeong Son [3], Van Luong Nguyen [2], Tae-Soo Lim [2], Dong-Yeol Yang [2], Min-Hyeong Kim [2], Ki Bong Kim [2], Young Ja Kim [2], Jun Hong Lee [2], Yang Do Kim [1], Inyoung Kim [3], Taik-Min Lee [3], Yong-Jin Kim [2] and Sangsun Yang [2,*]

1 School of Materials Science and Engineering, Pusan National University, Busan 46241, Korea; sanghooni79@kims.re.kr (S.H.K.); yangdo@pusan.ac.kr (Y.D.K.)
2 Powder Technology Department, Korea Institute of Materials Science, Changwon 51508, Korea; luongnv@kims.re.kr (V.L.N.); lts6122@kims.re.kr (T.-S.L.); dyyang@kims.re.kr (D.-Y.Y.); mhkim@kims.re.kr (M.-H.K.); cyrano123@kims.re.kr (K.B.K.); kimyj12@kims.re.kr (Y.J.K.); junehong1027@kims.re.kr (J.H.L.); yjkim@kims.re.kr (Y.-J.K.)
3 Deparment of Printed Electronics, Korea Institute of Machinery and Materials, Daejeon 34103, Korea; ojhdsrd@kimm.re.kr (M.J.S.); ikim@kimm.re.kr (I.K.); taikmin@kimm.re.kr (T.-M.L.)
* Correspondence: nanoyang@kims.re.kr; Tel.: +82-055-280-3517

Academic Editor: Hugo F. Lopez
Received: 28 January 2016; Accepted: 4 March 2016; Published: 25 March 2016

Abstract: Three kinds of Bi-based solder powders with different chemical compositions of binary Bi–Sn, ternary Bi–Sn–In, and quaternary Bi–Sn–In–Ga were prepared using a gas atomization process and subsequently ball-milled for smaller-size fabrication. In particular, only the quaternary Bi–Sn–In–Ga solder powders were severely broken to the size of less than 10 μm in a polyhedral shape due to the presence of the constitutional element, the degree of overall oxidation, and the formation of solid solution, which had affected the fractured extent of the Ga-containing solder powders. Furthermore, a melting point also decreased by the addition of In and/or Ga into the binary Bi–Sn solder system, resulting in a melting point of 60.3 °C for the Bi–Sn–In–Ga solder powders. Thus, it was possible that fractured Bi–Sn–In–Ga solder powders were appropriate for the adhesion of more compact solder bump arrays, enabling reflowing at the low temperature of 110 °C on a flexible polyethylene terephthalate (PET) substrate.

Keywords: Ga-containing solder; ball milling; PET (polyethylene terephthalate) substrate; solder bump; solid solution

1. Introduction

Fabricating small-sized solder powders is an essential approach to constituting more compact solder bump arrays, because the solder bump size on a packaging substrate decreases as a result of the miniaturization of electronic components, and the pitch distance drops to the submicron level [1,2]. Although gas-atomized solder powders are several tens of micrometers small, even smaller solder powders are required to meet the demands of more advanced solder bumps for high microelectronic package loading [3–6]. In addition to the gas atomization process, a facile ball-milling process can be used for fabricating smaller-sized solder powders [7]. However, this method, which imparts high impact energy, can only be applied to brittle materials and is limited to ductile solder powders [7]. As an alternative, some brittle materials such as Bi, Ga, and Ge can be added to the solder powders, making the solder alloy more brittle, and these more brittle solder powders can be ball-milled to reduce their size [8–10]. Meanwhile, Bi-based solder powders are widely used in interconnection applications on glass or metallic substrates with regard to several advantages of good solderability, reasonable cost, and low melting point [10]. During alloy formation, the Bi solder constituent reacts with the

others to form various intermetallic compounds (IMCs) [10]. Since most IMCs are brittle, excessive IMCs can allow solder powders to be ball-milled. Among various supplementary elements, Ga has received great attention as its utility as a solder additive due to its tremendous properties such as an intrinsic low melting point and the ability to impart brittleness to the employed materials [8]. Ga easily alloys with many other solder elements by diffusing into their lattice, and Ga diffuses into the grain boundaries of other solder alloys, making them very brittle [11]. Lin *et al.* reported that the Ga-containing Bi–Sn–*x*Ga solder possesses high ductility resistance, because the Ga-rich phases at the grain boundaries are believed to impede grain growth [12].

Besides the fabrication of small-sized solder powders, demand has increased for advanced solder bumps reflowed on a flexible plastic substrate [13]. This has created a need to lower solder melting points so that the flexible plastic substrate is not damaged during reflow soldering [14]. This challenge can be simply solved by dissolving supplementary elements in conventional solder. For example, the addition of third, or even fourth elements such as Bi, In, and Ga into eutectic Sn–9Zn solder with a melting point of 198 °C can significantly lower the melting point, depending on the amount of the solder additive employed [11,15,16]. Notably, In has very high solubility with other solder elements, and thus can provide a sharp melting point depression (e.g., eutectic In–48Sn solder with a melting point of 118 °C) [17]. However, there still remains a need to find a suitable substitute, due to the high cost issue [17]. Relatively, Ga can offer economic advantages over In as an additive to effectively lower the melting point of the solder alloy. Although such In and Ga solder additives are not currently popular for microelectronic packaging on metallic or ceramic substrates, they present interesting compositions for obtaining reliable, economical solder joints for interconnection applications on flexible plastic substrates.

Herein, three different types of Bi-based solder powders that have chemical compositions of binary Bi–Sn, ternary Bi–Sn–In, and quaternary Bi–Sn–In–Ga solder powders are investigated in respect of their thermal behavior, microstructural phase, mechanical strength, and reflow solderability; in particular, the presence of specific IMCs in the Bi–Sn–In–Ga solder powders have significantly influenced the breakage of the solder powders (the size of less than 10 μm) when using the ball-milling process. Then, the melting point of the Ga-containing solder powders is significantly lowered to 60.3 °C. As a result, the solder pastes that consist of a mixture of ball-milled Bi–Sn–In–Ga solder powders and epoxy resins are reflowed on the PET substrate at the low temperature of 110 °C, because the flexible plastic film will not be damaged at this temperature [14].

2. Materials and Methods

Bismuth pieces (Bi, 99.999%), tin shots (Sn, 99.8%), indium pieces (In, 99.99%), and gallium (Ga, 99.99%) were obtained from Sigma Aldrich, St. Louis, MO, USA. Three different types of Bi-based solder powders that have specific chemical compositions of binary Bi–Sn, ternary Bi–Sn–In, and quaternary Bi–Sn–In–Ga, as shown in Table 1, were fabricated using a gas atomizer (Hot Gas Atomization System, PSI Ltd., Hailsham, East Sussex, UK) under identical conditions. The gas atomization process was commenced by melting of 1.0 kg of the solder elements in a graphite crucible, at 400 °C for 10 min. The molten solder liquid was then readily atomized to form small droplets and rapidly solidified due to the heat convection in the surrounding gas flow of 30 bar. After all these processes, the gas-atomized solder powders were collected and thereafter loaded onto a series of American Society for Testing and Materials (ASTM) E11 standard sieves and shaken on a sieve shaker for 10 min to obtain the solder powders within the specific size range of 26–38 μm. The Bi-based solder powders were ball-milled within a stainless steel jar with zirconia balls to obtain solder powders with less than the initial size that were obtained when using planetary ball-milling equipment (ARE-310, Dongwhan, Seoul, Korea). The planetary motion of 220 rpm threw the balls strongly against each other, and thus the quaternary Bi–Sn–In–Ga solder powders were severely broken to the size of less than 10 μm. The fractured solder powders were blended with epoxy resins at a 95:5 weight percentage ratio using a three-roll miller (EXAKT 50 I, EXAKT Technologies, Inc., Oklahoma City, OK, USA), to

make the solder pastes. The specimens were patterned with dot arrays of dimensions 50 mm × 50 mm on the polyethylene terephthalate (PET) substrate and were prepared using a custom-made screen printer; it was then reflowed at 110 °C in a glove box filled with an inert gas. Practically, the ball-milled Bi–Sn–In–Ga solder pastes should be deposited on the surface-modified PET, such as Cu-sputtered PET, indium tin oxide (ITO)-coated PET, or conductive polymer-coated PET, to ensure more realistic conditions and better electron flow between microelectronics and substrates. In the present study, however, we mainly focused on solder materials rather than plastic substrates. Thus, they were just reflowed on the raw PET substrate to show the practical reflow possibility of novel solder pastes and to determine the damage extent of the PET, even at such a low soldering temperature.

Table 1. Chemical compositions, O amounts, and intermetallic compounds (IMCs) of Bi-based solder powders prepared by a gas atomization process.

Bi (wt.%)	Sn (wt.%)	In (wt.%)	Ga (wt.%)	O (wt.%)	IMCs
58.0	42.0	–	–	0.0987	No IMCs
43.5	31.5	25.0	–	0.0884	In0.2Sn0.8 & BiIn
41.4	30.0	23.8	4.8	0.0593	In0.2Sn0.8, Ga0.9In0.1, & BiIn

The concentration of oxygen contained in the solder powders was determined using an O/N analyzer (ON–900, ELTRA GmbH, Haan, Germany). The microstructure image and chemical composition of the gas-atomized solder powders, the cross-sectional solder alloys, and the solder pastes on the PET substrate before and after reflow were acquired using a scanning electron microscope (SEM, JSM–5800, JEOL, Tokyo, Japan). The constitutional elements and IMCs of Bi-based solder powders were determined by an X-ray diffraction spectroscope (XRD, D/Max-2500VL/PC, Rigaku International Corporation, Tokyo, Japan). Their thermal properties were measured using a differential scanning calorimeter (DSC, Q600, TA Instrument, New Castle, DE, USA). The Bi-based solder alloy was heat-treated into an alumina crucible at about 400 °C, and the ingot was then shaped into a tensile-strength testing sample (2.00 mm wide × 4.58 mm thick). A tensile testing machine (Universal Testing Machine 4485, Instron, Norwood, MA, USA) was used.

3. Results and Discussion

The surface morphologies of Bi-based solder powders within the same size range of 26–38 μm are shown in Figure 1. As shown in Figure 1a, it was found that the Sn–Bi solder powders had rough spherical shapes, composed by each major Bi-rich phase and minor Sn-rich phase, because there were no IMCs between the two phases. In the surface image of the Bi–Sn–In solder powders (Figure 1b), there were residual areas that had an In-rich phase embedded in the interfacial boundaries; it was considered that the In bridged between Bi and Sn, and thus formed Bi–In and In–Sn IMCs. However, there were distinguishable thick layer phases in the Bi–Sn–In–Ga solder powders (Figure 1c), and the XRD analysis revealed that the induced phases were composed of Ga-rich and In-rich phases in the Bi–Sn solder system; thus, it predicated on the formation of Ga0.9In0.1, BiIn, and In0.2Sn0.8 IMCs according to the Ga–In, Bi–In, and In–Sn interfacial reactions. Since the IMCs were usually brittle, the overall ductility of the solder joints was decreased, which allowed ball-milling for finer-size fabrication.

Figure 1d shows the X-ray diffraction patterns of binary Bi–Sn, ternary Bi–Sn–In, and quaternary Bi–Sn–In–Ga solder powders. Each Bi and Sn phase appears in the XRD pattern of the Bi–Sn solder powders, but there were no peaks of IMCs between Bi and Sn [18]. However, the addition of In in the Bi–Sn solder system resulted in the occurrence of new peaks of BiIn and In0.2Sn0.8 IMCs; thus, In took a bridging role between Bi and Sn [18]. Moreover, the addition of Ga in the Bi–Sn–In solder system formed further occurrences of peaks of the solid solutions between In and Ga, Ga0.9In0.1, which was in correspondence to the Joint Committee on Powder Diffraction Files (JCPDF) No. 34–1437. As a result, while Bi–Sn solder powders had no IMCs, the addition of In and Ga formed significant amounts

of various Ga–In, Bi–In, and In–Sn IMCs, which made the Bi–Sn–In–Ga solder powders very brittle, thus allowing ball-milling for finer-size fabrication.

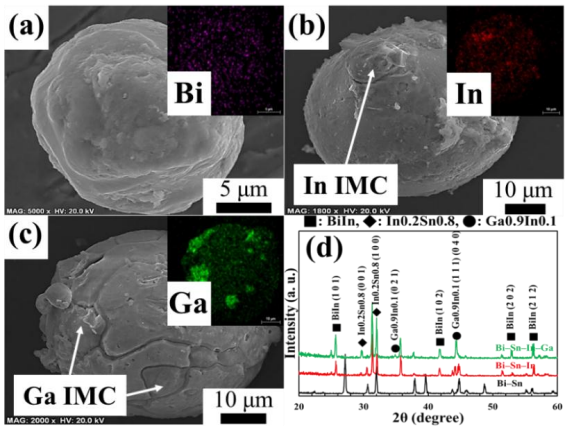

Figure 1. SEM images and elemental mapping results (the inset of each image) of (**a**) a binary Bi–Sn powder with the inset of Bi-rich phase; (**b**) a ternary Bi–Sn–In powder with the inset of In-rich phase and (**c**) a quaternary Bi–Sn–In–Ga solder powder with the inset of Ga-rich phase. XRD analysis results (**d**) of Bi-based solder powders.

Each microstructure of the as-raw and ball-milled Bi–Sn–In–Ga solder powders was shown in Figure 2. The planetary motion threw the balls against each other strongly generating high impact energy; thus, the quaternary Bi–Sn–In–Ga solder powders were severely broken and fragmented during the operation time as the fracture control parameter. Since the rotational speed of the ball-milling process was optimized to reduce the size of the solder powders, their fractured extent was controlled by changing the running time as the control parameter. However, as the running time increased, the amount of fractured solder powders increased, and the average size was significantly decreased as an effect of ball-milling. For the Bi–Sn–In–Ga solder powders before the ball-milling process, a definitely layered morphology along the interface is shown in Figure 1c, the higher magnification image of Figure 2a. In contrast, it was possible to observe an agglomerated morphology (Figure 2d) on the surface of the fractured solder powders.

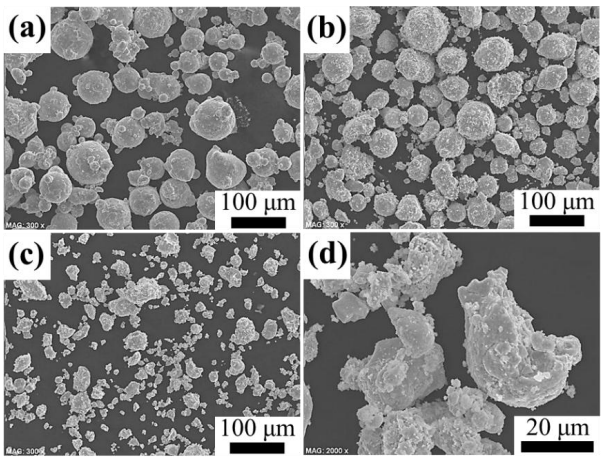

Figure 2. SEM images of fractured Bi–Sn–In–Ga solder powders in different operation time: (**a**) no ball-milling; (**b**) ball-milled for 30 min, and (**c**) ball-milled for 4 h. High magnification of SEM images: (**d**) ×2000.

Figure 3 shows the microstructure and chemical composition of the investigated Bi–Sn–In–Ga solder powders. Figure 3a shows the fractured solder powders with rugged surface structure. In the elemental mapping analysis (Figure 3b–e), Sn overlapped together with In, referred to as In0.2Sn0.8 IMC, and there was a broad distribution of Ga, which informed the formation of a specific Ga0.9In0.1 IMC between In and Ga. Furthermore, energy-dispersive X-ray spectroscopy (EDS) analysis (Figure 3f) on the surface of the fractured solder powders demonstrated the significant increase of Ga content compared to the Ga content of the as-raw solder powders before ball-milling. The chemical composition of the fractured Ga-containing solder powders was identified as 37.53 wt.% Bi, 26.88 wt.% Sn, 27.46 wt.% In, and 2.65 wt.% Ga; then, the O amount drastically increased from 2.62 to 5.48 wt.%, which indicated that the spalled solder powders were severely oxidized during ball-milling, and the subsequent oxidized solder powders became more brittle to be broken and spalled for finer-size fabrication. As a result, the Ga-rich phase was segregated in the vicinity of the interfacial boundaries of the Bi–Sn solder system; thereafter, the Ga-containing solder powders were fractured along the brittle Ga-rich phase during the ball-milling process. It was quite spectacular to notice that, unlike conventional Bi-based and Sn-based solder powders with high ductility, the Ga-containing solder powders were ball-milled to become finer-sized, although the spalled solder powders were mostly polyhedral shapes.

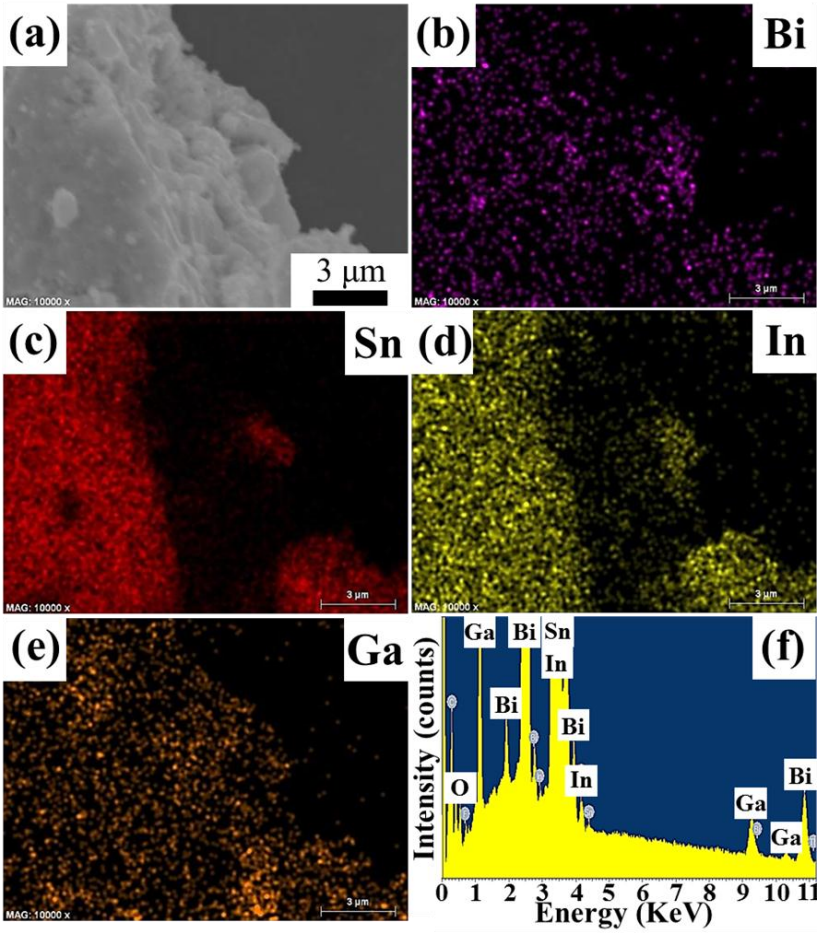

Figure 3. Fractured surface SEM images of ball-milled Bi–Sn–In–Ga solder powders. Mapping analysis results: (**b**) for Bi, (**c**) for Sn, (**d**) for In, and (**e**) for Ga. EDS analysis (**f**) on the surface of (**a**): the amount of Ga emitted on the fractured surface significantly increased.

Fractured Bi–Sn–In–Ga solder powders with a size of less than 10 μm were successfully fabricated via a combination of gas atomization and ball milling. The schematics of the quaternary Bi–Sn–In–Ga solder powders containing many IMCs and the ball-milling process are shown in Figure 4. After

Ga was added in the Bi–Sn–In solder system, the Bi–Sn–In–Ga solder powders were well fractured during the ball-milling process due to the precipitation of many different IMCs at the interfacial boundary. However, when the same process was applied to the Bi–Sn and Bi–Sn–In solder powders, they appeared and developed into a consolidated, agglomerated bulk due to their remaining ductile conditions according to the formation of less IMCs. In other words, only Ga-containing solder powders were broken across solid solutions at the interfacial boundaries by the cascaded zirconia balls with high impact energy during the ball-milling process. Then, both the size and shape of the solder balls were significantly changed after the ball-milling process, but most properties except for their polyhedral shape and the average size were similar to those of the as-raw, gas-atomized solder powders. After the fractured solder powders were well blended with epoxy resins, they were directly patterned on the PET substrate as actual solder pastes for any post-processing.

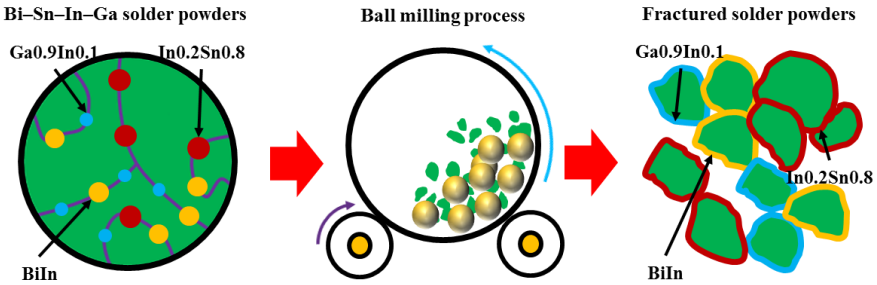

Figure 4. The ball-milling effect of quaternary Bi–Sn–In–Ga solder powders induced from the formation of brittle IMCs.

The DSC curves in Figure 5 show the thermal behavior of Bi-based solder powders. The prominent endothermic peak of the Bi–Sn–In solder powders shifted to 82.0 °C from the Bi–Sn solder powders having a peak at 139.6 °C when the content of In was increased to 23.8 wt.%. Continuously, the addition of 4.8 wt.% Ga shifted the peak even more, to 60.3 °C. Thus, the addition of an appropriate amount of In and Ga shifted the endothermic peak to the pre-determined melting point of the solder powders. It is noteworthy that a slight shoulder was observed on the left side of the melting point peak for the Bi–Sn–In solder powders. The appearance of the shoulder is a result of the formation of an In-rich phase. The addition of 4.8 wt.% Ga into the Bi–Sn–In solder system also resulted in the formation of various Ga0.9In0.1, BiIn, and In0.2Sn0.8 IMCs. Because such solid solutions have relatively high melting points due to their covalent bonds, the melting ranges of the Bi–Sn–In and the Bi–Sn–In–Ga solder powders became broader [19].

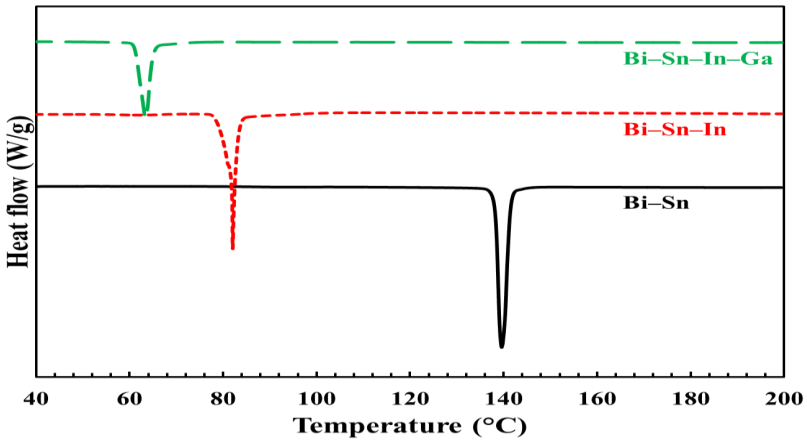

Figure 5. DSC of Bi-based solder powders.

The average yield strength (Figure 6) of the Bi–Sn solder alloy remained constant at 40.1 MPa, having a standard deviation of 1.8 MPa. However, the yield strength drastically dropped to 10.2 MPa as the In and Ga content were increased to 4.8 and 23.8 wt.%, respectively. The average ultimate tensile strength of the solder alloy simultaneously decreased from 49.8 to 16.6 MPa when both In and Ga were added to the Bi–Sn solder system. Afterwards, the average elongation decreased from 9.5% to 1.8% as the concentrations of In and Ga increased. The Bi–Sn–In–Ga solder alloy containing 4.8 wt.% Ga and 23.8 wt.% In exhibited very low tensile strength values compared to the Bi–Sn solder alloy. In particular, the Bi–Sn–In–Ga solder alloy had average elongation as low as 1.8%. This comparison indicates that the addition of In and/or Ga into the solder alloy significantly deteriorated the tensile strength values and significantly reduced the solder alloy ductility, as induced by the formation of various IMCs [20]. Overall, the tensile strength values of the Ga-containing solder alloy were much smaller than those of the Bi–Sn solder alloy. This phenomenon also reflected a significant decrease in the solder alloy ductility upon increasing the amount of In and Ga, induced from the formation of IMCs with them. As a result, the comparison of ductility for three kinds of solders indicates the adequate performance of Bi–Sn–In–Ga solder alloy, as realized from its appropriate level of elongation when considered at strain rate levels.

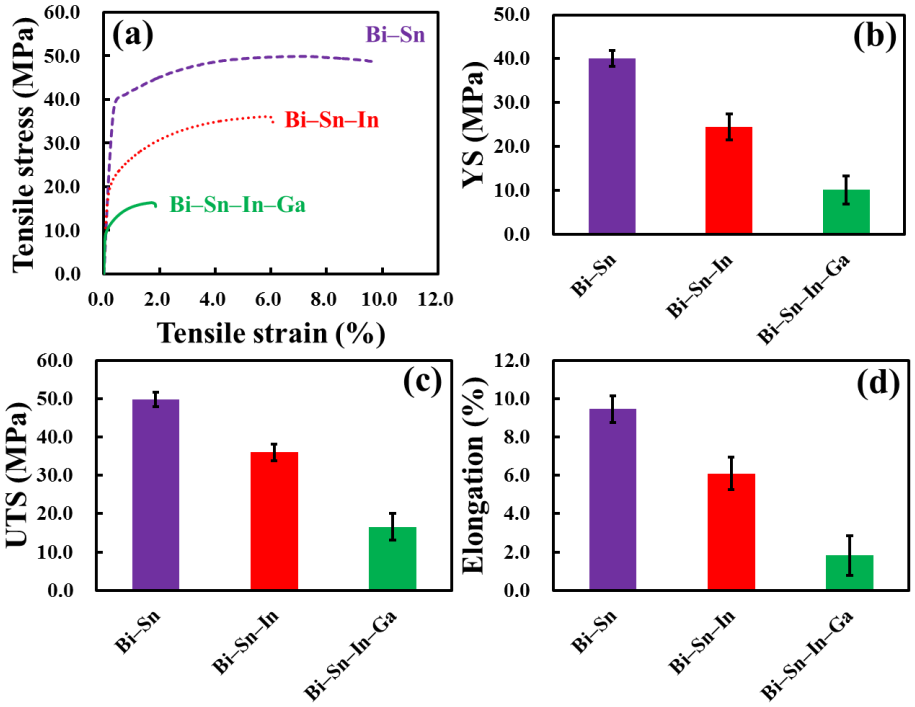

Figure 6. Tensile strength measurements of Bi-based solder alloys. Strain-stress curves (**a**) were taken from representative single samples, which are different from the average results. The other graphs represent the average and standard deviation values of each yield strength (**b**), ultimate tensile strength (**c**) and elongation (**d**) of the Bi-based solder alloys.

Figure 7a shows the screen-printed pattern of Ga-containing solder pastes on the square PET substrate prior to reflow. After being printed, the solder pastes were successfully attached without creating links between neighboring solder bumps. In addition, the shape uniformity of the solder pastes was well-controlled by the blockage mold and the pitch distance between solder bumps was 700 μm. Actually, Figure 7b,c show the consolidated, agglomerated Bi–Sn–In–Ga solder powders prior to reflow soldering. Since the hydrophobic epoxy resins were well mixed with fractured Bi–Sn–In–Ga solder powders to prevent oxidation during reflow soldering, they contributed to the adhesion stability and thermal wettability on the flexible plastic substrate [21]. After the reflow soldering process at the

low temperature of 110 °C, the bump morphology changed its shape to spherical from polyhedral shape, and the surface of the solder bumps became smoother as shown in Figure 7d,e. This surface modification was ascribed to the high solderability of Ga-containing solder powders. As shown in Figure 7e, the solder powders reflowed on the raw PET substrate demonstrated poor wettability due to the heterojunction between metallic solder powders and organic polymer substrates (metal-organic interfaces). In general, conventional Cu pads are used in practical soldering applications, because they provide good wettability to the reflowed solder powders, forming specific IMCs between metallic solder powders and Cu substrates, such as Cu_6Sn_5 and Cu_3Sn. Thus, the PET should be coated with conductive metals or ceramics, such as copper, gold, silver, platinum, or indium tin oxide (ITO), to enhance the wettability of the solder powders. However, the main scope of this present study is to fabricate smaller-sized solder powders using a facile ball-milling process and to reflow the solder powders on the plastic substrate. Thus, the actual use and the practical application of the surface-modified PET substrate were omitted, because the focus is simply to determine the soldering possibility (solderability and reflowability) of ball-milled solder powders on the PET and the degree of thermal damage of the PET, even at such a low soldering temperature. Overall, the fractured solder powders with flux also consolidated toward the center upon reflow soldering. Subsequently, the solder bumps became bendable and stretchable after they were reflowed to the PET substrate, which was then applied to flexible devices as shown in Figure 7f. As a result, the as-reflowed spherical solder bumps were distributed, but the small size of the solder bumps were dispersed around the main solder bumps and were strongly bonded on the PET substrate.

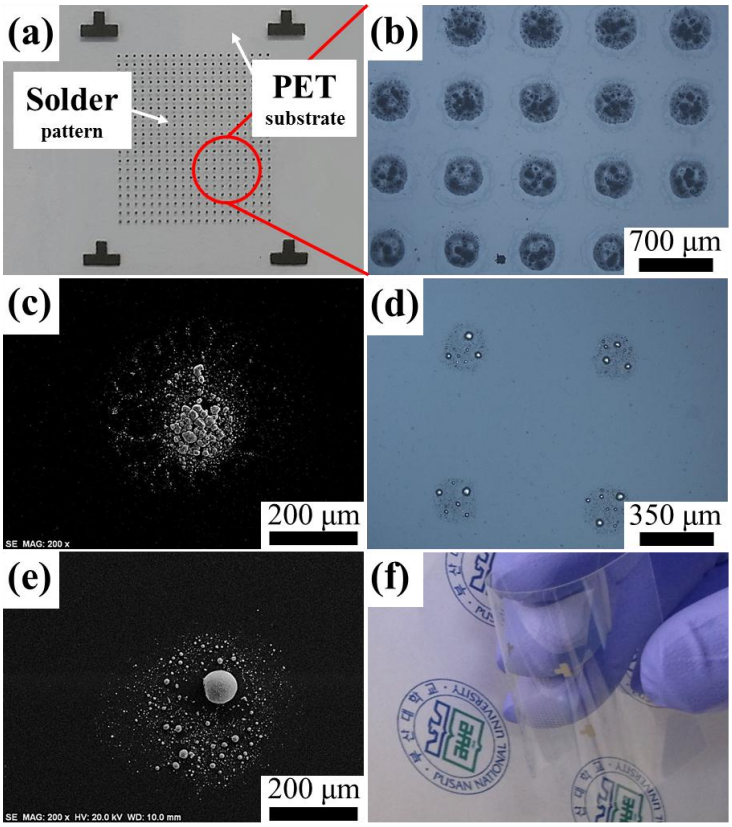

Figure 7. Feasibility test for Bi–Sn–In–Ga solder pastes. Screen-printed patterns (**a**) of the solder pastes prior to reflow; OM image (**b**) of the solder patterns prior to reflow, having a pitch distance of 700 μm; SEM image (**c**) of the solder pastes prior to reflow; OM image (**d**) of the solder bumps after reflow; SEM image (**e**) of the solder bumps after reflow; a photograph (**f**) of solder bumps on a PET substrate with flexibility and bendability after reflow.

4. Conclusions

The microscopic, spectroscopic, and physical properties of three kinds of Bi-based solder powders with different chemical compositions of binary Bi–Sn, ternary Bi–Sn–In, and quaternary Bi–Sn–In–Ga were compared. In particular, the microscope images showed that the surface morphology of the Bi-based solder powders had become more intergranular, due to the formation of more IMCs in accordance with the addition of In and/or Ga in the binary Bi–Sn solder system. Furthermore, the addition of Ga in the Bi–Sn–In solder system significantly increased the brittleness in the Bi–Sn–In–Ga solder powders, which made ball-milling for the fabrication of finer-sized solder powders with less than 10 μm possible. Subsequently, the addition of supplementary elements to the binary Bi–Sn solder system also drastically decreased the melting point of the solder powders by shifting to a eutectic composition with a lower temperature, which allows the ball-milled Bi–Sn–In–Ga solder powders to reflow on a flexible film at the low temperature of 110 °C.

Acknowledgments: We are grateful for the financial support from the R&D Convergence Program of MSIP (Ministry of Science, ICT and Future Planning) and the ISTK (Korea Research Council for Industrial Science and Technology) of Republic of Korea (Grant B551179-12-02-00). This work was also supported by the Electronics and Telecommunications Research Institute (ETRI).

Author Contributions: Sang Hoon Kim conceived and designed the experiments; Min Jeong Son, Tae-Soo Lim, Min-Hyeong Kim, Ki Bong Kim, Young Ja Kim and Jun Hong Lee performed the experiments; Van Luong Nguyen, Dong-Yeol Yang, Inyoung Kim and Taek-Min Lee analyzed the data; Taek-Min Lee, Yang Do Kim and Yong-Jin Kim wrote the paper; Sangsun Yang edited the paper.

Conflicts of Interest: The authors declare no conflict of interest.

Abbreviations

The following abbreviations are used in this manuscript:

PET:	Polyethylene Terephthalate
IMC:	Intermetallic Compound
ASTM:	American Society for Testing and Materials

References

1. Huang, M.; Zhao, J.; Zhang, Z.; Zhao, N. Role of diffusion anisotropy in β-Sn in microstructural evolution of Sn-3.0 Ag-0.5 Cu flip chip bumps undergoing electromigration. *Acta Mater.* **2015**, *100*, 98–106. [CrossRef]
2. Chan, Y.C.; Yang, D. Failure mechanisms of solder interconnects under current stressing in advanced electronic packages. *Prog. Mater. Sci.* **2010**, *55*, 428–475. [CrossRef]
3. Ji, H.; Qiao, Y.; Li, M. Rapid formation of intermetallic joints through ultrasonic-assisted die bonding with Sn-0.7 Cu solder for high temperature packaging application. *Scr. Mater.* **2016**, *110*, 19–23. [CrossRef]
4. Chu, K.; Sohn, Y.; Moon, C. A comparative study of Cn/Sn/Cu and Ni/Sn/Ni solder joints for low temperature stable transient liquid phase bonding. *Scr. Mater.* **2015**, *109*, 113–117. [CrossRef]
5. Plookphol, T.; Wisutmethangoon, S.; Gonsrang, S. Influence of process parameters on SAC305 lead-free solder powder produced by centrifugal atomization. *Powder Technol.* **2011**, *214*, 506–512. [CrossRef]
6. Minagawa, K.; Kakisawa, H.; Osawa, Y.; Takamori, S.; Halada, K. Production of fine spherical lead-free solder powders by hybrid atomization. *Sci. Technol. Adv. Mater.* **2005**, *6*, 325–329. [CrossRef]
7. Tang, W.; Zhang, H.; Wu, Y.; Zheng, Z. Mechanical alloying synthesis and soldering microstructures of nanocrystalline Sn-3.5 Ag-0.7 Cu alloy powders. *J. Alloy. Compd.* **2010**, *497*, 396–401. [CrossRef]
8. Liu, N.; Lin, K. The effect of Ga content on the wetting reaction and interfacial morphology formed between Sn-8.55 Zn-0.5 Ag-0.1 Al-xGa solders and Cu. *Scr. Mater.* **2006**, *54*, 219–224. [CrossRef]
9. Wang, S.; Chin, T.; Yang, C.; Chen, S.; Chuang, C. Pb-free solder-alloy based on Sn–Zn–Bi with the addition of germanium. *J. Alloy. Compd.* **2010**, *497*, 428–431. [CrossRef]
10. Mahdavifard, M.; Sabri, M.; Shnawah, D.; Said, S.; Badruddin, I.; Rozali, S. The effect of iron and bismuth addition on the microstructural, mechanical, and thermal properties of Sn-1Ag-0.5 Cu solder alloy. *Microelectron. Reliab.* **2015**, *55*, 1886–1890. [CrossRef]

11. Mohanty, U.S.; Lin, K. The effect of alloying element gallium on the polarization characteristics of Pb-free Sn–Zn–Ag–Al–XGa solders in NaCl solution. *Corros. Sci.* **2006**, *48*, 662–678. [CrossRef]
12. Lin, S.; Nguyen, T.L.; Wu, S.; Wang, Y. Effective suppression of interfacial intermetallic compound growth between Sn-58 wt.% Bi solders and Cu substrates by minor Ga addition. *J. Alloy. Compd.* **2014**, *586*, 319–327. [CrossRef]
13. Akin, M.; Rissing, L.; Pichler, E. Design guidelines for efficient eutectic soldering onto low Tg polymeric multimode light waveguides. *Procedia Technol.* **2014**, *15*, 168–177. [CrossRef]
14. Zardetto, V.; Brown, T.M.; Reale, A.; Di Carlo, A. Substrates for flexible electronics: A practical investigation on the electrical, film flexibility, optical, temperature, and solvent resistance properties. *J. Polym. Sci. Part B Polym. Phys.* **2011**, *49*, 638–648. [CrossRef]
15. Nazeri, M.F.M.; Mohamad, A.A. Corrosion resistance of ternary Sn-9Zn-xIn solder joint in alkaline solution. *J. Alloy. Compd.* **2016**, *661*, 516–525. [CrossRef]
16. Ahmido, A.; Sabbar, A.; Zouihri, H.; Dakhsi, K.; Guedira, F.; Serghini-Idrissi, M.; El Hajjaji, S. Effect of bismuth and silver on the corrosion behavior of Sn-9Zn alloy in NaCl 3 wt.% solution. *Mater. Sci. Eng. B* **2011**, *176*, 1032–1036. [CrossRef]
17. Shu, Y.; Rajathurai, K.; Gao, F.; Cui, Q.; Gu, Z. Synthesis and thermal properties of low melting temperature tin/indium (Sn/In) lead-free nanosolders and their melting behavior in a vapor flux. *J. Alloy. Compd.* **2015**, *626*, 391–400. [CrossRef]
18. Shalaby, R.M. Effect of silver and indium addition on mechanical properties and indentation creep behavior of rapidly solidified Bi–Sn based lead-free solder alloys. *Mater. Sci. Eng. A* **2013**, *560*, 86–95. [CrossRef]
19. Kotadia, H.R.; Howes, P.D.; Mannan, S.H. A review: On the development of low melting temperature Pb-free solders. *Microelectron. Reliab.* **2014**, *54*, 1253–1273. [CrossRef]
20. Zhang, Q.; Long, W.; Yu, X.; Pei, Y.; Qiao, P. Effects of Ga addition on microstructure and properties of Sn–Ag–Cu/Cu solder joints. *J. Alloy. Compd.* **2015**, *622*, 973–978. [CrossRef]
21. Mustafa, M.; Suhling, J.C.; Lall, P. Experimental determination of fatigue behavior of lead free solder joints in microelectronic packaging subjected to isothermal aging. *Microelectron. Reliab.* **2016**, *56*, 136–147. [CrossRef]